

## Regeneration ability of acute liver injury after bee sting was observed by early hepatic microperfusion changes

Shifeng Lai<sup>1,2</sup>, Jinlian Li<sup>1,2</sup>, Qinglan He<sup>2</sup>, Mingxing LI<sup>1</sup>

<sup>1</sup>Department of Ultrasound, The Affiliated Hospital of Southwest Medical University, Luzhou 646000, China

<sup>2</sup>Department of Ultrasound, Jianyang People's Hospital, Jianyang 641400, China

**Introduction.** To construct a rat model of melittin-induced acute liver injury (ALI) and investigate the relationship between microcirculation blood perfusion changes, as evaluated via contrast-enhanced ultrasound (CEUS), and the mechanism underlying the inflammatory changes in bee sting-induced ALI.

**Methods.** In the present study, a rat model of ALI caused by bee sting was constructed. CEUS parameters, serological tests, histopathologic examination, and mRNA expression of inflammatory factors were measured in the group of 0h after injection of normal saline and 6, 12, 24 h after injection of mellitoxin groups.

**Results.** The CEUS parameters were significantly higher in the 6H, 12H, and 24H groups. Interleukin (IL)-6, nuclear factor kappa B (NF- $\kappa$ B) and signal transducer and activator of transcription (STAT3) expression increased at 12 and 24 h. A positive correlation between STAT3 and peak intensity, area under the curve (AUC), and mean transition time (MTT) in the 6H group but a negative correlation between ALT and MTT and AUC in the 6H group.

**Conclusions.** CEUS quantitative evaluation of micro-perfusion changes in bee sting can observe the regeneration ability after ALI, and provide new ideas for clinical diagnosis and treatment of bee sting.

**Keywords.** Melittin, Contrast-enhanced ultrasound, Acute liver injury, Perfusion, Regeneration.

### 1 INTRODUCTION

Bee venom is a complex mixture with neurotoxic and immunogenic properties<sup>[1]</sup>, including the primary component melittin, other peptides, enzymes, and biogenic amines<sup>[2]</sup>. Once bee venom enters the human body, it will result in allergic reactions<sup>[3]</sup>,

thrombocytopenia, microcirculation disturbance, and liver and kidney function damage<sup>[4]</sup>. Approximately 46.6% of such individuals develop acute toxic hepatitis<sup>[5]</sup>, possibly inducing structural and functional liver damage as well as acute liver failure (ALF)<sup>[6]</sup>.

In liver injury after bee sting poisoning, serum biochemical changes primarily manifest as an increase in aspartate aminotransferase (AST) or alanine aminotransferase (ALT) levels<sup>[3]</sup>. Histopathologic examination has revealed inflammatory cell infiltration, disordered hepatic lobule arrangement, diffuse hepatocyte degeneration, and hepatocyte degeneration or necrosis<sup>[1]</sup>. Furthermore, during hepatocyte injury, proinflammatory factors and inflammatory pathways are abnormally activated<sup>[7]</sup>. Interleukin (IL)-6, an important proinflammatory factor in acute liver injury (ALI)<sup>[8]</sup>, was significantly increased in a mouse ALI model<sup>[9, 10]</sup>. IL-6 upregulation in ALI results in the rapid activation of the transcription factors nuclear factor kappa B (NF- $\kappa$ B) and signal transducer and activator of transcription 3 (STAT3)<sup>[10]</sup>; this activation plays a vital role in toxin clearance and hepatocyte regeneration<sup>[11, 12]</sup>. In addition, liver microcirculation disorders play a vital role in ALI pathogenesis<sup>[13]</sup>. Moreover, inflammation can promote liver microcirculation dysfunction and is a determinant of liver injury<sup>[14]</sup>.

Contrast-enhanced ultrasound (CEUS) is a type of imaging technique<sup>[15]</sup> in which intravascular signals are enhanced by intravenously injecting a contrast agent<sup>[13]</sup>. By analyzing the peak intensity (PI), time to peak (TTP), mean transition time (MTT), and area under the curve (AUC) of the contrast agent in the region of interest (ROI), microvascular blood flow can be quantitatively detected, changes in liver hemodynamics can be dynamically observed, and changes in liver microcirculation can be identified early<sup>[16]</sup>. At present, CEUS is widely used for liver cancer<sup>[17]</sup>, ALF<sup>[18]</sup>, liver fibrosis<sup>[19]</sup>, animal models of acute liver reperfusion injury<sup>[20]</sup>, and liver transplantation<sup>[21]</sup>.

At present, studies on the changes in liver microvascular dysfunction, proinflammatory factors, and inflammatory regulatory factors and their interaction mechanisms during bee sting-induced ALI are limited. Therefore, in this study, we elucidated the mechanisms underlying microcirculation blood perfusion and inflammatory changes in bee sting-induced

liver injury by constructing a melittin-induced ALI model to analyze the application value of CEUS in bee sting-induced ALI and decrease ALF occurrence.

## 2 MATERIALS AND METHODS

### 2.1 Animal grouping

Thirty-two male Sprague Dawley rats (weighing  $300 \pm 50$  g) were purchased from Chengdu Dashuo Experimental Co., Ltd. They were adaptively fed in a 12 h light/dark environment for 3 days in an animal room maintained at a 25°C temperature and 40%–70% humidity. The rats were randomly divided into four groups (eight rats in each group): control (0H), melittin injection at 6 h (6H), melittin injection at 12 h (12H), and melittin injection at 24 h (24H) groups. The Department of Laboratory Animal Resources and the Animal Research Ethics Committee of Southwest Medical University approved this study (SWMU20210393) and all methods were carried out in accordance with relevant guidelines and regulations.

### 2.2 Animal model

After subjecting the rats to fasting and water deprivation for 12 h, they were anesthetized by intraperitoneally injecting 1% pentobarbital (50 mg/kg). After the disappearance of the pain reflex, the rats were fixed on an operating table in the supine position. Hemostatic forceps were used to pull out the tongue. Then, iodophor solution was used to prepare and sterilize the entire abdomen. Under ultrasound guidance, a 24G indwelling needle was inserted into the common femoral vein of the right hind leg of each rat. Based on the findings of a previous study<sup>[22]</sup> and preliminary experiments, the rats in the 6H, 12H, and 24H groups were administered 4  $\mu\text{g/g}$  melittin using the drainage tube of the indwelling needle and the time was recorded. Similarly, physiological saline was injected into the 0H group. When fully awake, the rats were returned to their cages and provided adequate food and water and a constant room temperature.

### 2.3 CEUS imaging

The livers from the four rat groups were subjected to CEUS imaging using an ultrasound diagnostic instrument (ACUSON S3000, Siemens, Germany). The rats in the four groups

were re-anesthetized, fixed in the supine position, and sterilized with iodophor solution, as described above. Under ultrasound guidance, a 24G indwelling needle was inserted into the common femoral vein of the left hind leg to establish a channel for injecting the ultrasound contrast agent. Two-dimensional and color Doppler ultrasounds were performed to observe the liver parenchyma and intrahepatic blood vessels; then, the appropriate liver parenchyma area without large blood vessels was selected. After fixing the section, CEUS was performed. The SonoVue<sup>®</sup> contrast agent (Bracco, Milan, Italy) was prepared in a microbubble suspension with 5 ml of 0.9% sodium chloride injection and injected into the left common femoral vein at a dose of 0.2 ml/kg. Finally, the tube was flushed with 0.5 ml of normal saline. The ultrasound instrument parameters were set according to the guidelines<sup>[23]</sup> as follows: mechanical index, 0.05; depth, 3.5 cm; gain, 0 dB; and frequency, 4 MHz. A 9L4 frequency conversion linear array probe was used to select a circular sampling area of 0.05 mm<sup>2</sup> as the ROI at the same depth and location in the right liver of rats. The 180-s dynamic data were acquired and stored in the Digital Imaging and Communications in Medicine (DICOM) format. A built-in analysis software of the ultrasound diagnostic instrument, auto-tracking contrast quantification, was utilized to quantitatively analyze the DICOM images, construct time–intensity curves (TICs), and obtain the following relevant parameters: PI, the maximum intensity of the contrast agent in the liver parenchyma; TTP, the time required to reach the peak intensity; MTT, the time required for the liver to exhibit a half peak washout intensity<sup>[21]</sup>; and AUC, the total amount of the contrast medium in the ROI during the examination<sup>[24]</sup>. The average of these parameters was utilized for further analysis. All parameters were measured three times by the same operator and the average value was used.

#### 2.4 Serological tests

After the rats were subjected to CEUS at the specified time points, 3 ml of inferior vena cava blood was collected and centrifuged at 3000 rpm for 5 min. Then, serum AST and ALT levels were measured using an automatic biochemical analyzer (BS-360S, Shenzhen Mindrai Biomedical Electronics Co., Limited, Shenzhen, China).

## 2.5 Total RNA extraction and quantitative real-time polymerase chain reaction (qRT-PCR)

After collecting blood samples, the rats were sacrificed by injecting air into the left common femoral vein. Thereafter, rat liver tissues were immediately removed and divided into two parts equally along the coronal plane: one part was stored in liquid nitrogen at  $-80^{\circ}\text{C}$  and the other was fixed with 10% neutral formaldehyde fixative. Total RNA was extracted from the liver tissues preserved in liquid nitrogen and subjected to qRT-PCR analysis using a previously described method<sup>[25]</sup>. First, the total RNA of liver tissues was extracted as a template. Then, the relative mRNA expression of IL-6, NF- $\kappa$ B, and STAT3 was measured in rats using the automatic medical PCR analysis system (SLAN-96S, Shanghai Hongshi Medical Technology Co., Ltd., China). GAPDH was used as the reference gene, and analysis was performed using the  $2^{-\Delta\Delta\text{CT}}$  method<sup>[26]</sup>. The results were obtained as fold changes for the 0H group. Table 1 lists the primer sequences used for real-time PCR analysis.

## 2.6 Histopathologic examination

The liver tissues fixed with 10% neutral formaldehyde fixative were removed, dehydrated using an alcohol gradient (75%–85%–90%–95%–100%), and then embedded with paraffin. The paraffin-embedded tissues were prepared using an embedding machine (JB-P5, Wuhan Junjie Electronics Co., Ltd., China) and sliced into 3  $\mu\text{m}$  thin slices. Hematoxylin–eosin staining was performed. Histopathologic changes were observed under a light microscope (Nikon Eclipse CI, Nikon, Japan) and images were collected. The entire procedure was performed by an experienced histopathologist who was blinded to the experimental procedure.

## 2.7 Statistical analysis

GraphPad Prism 8 (San Diego, CA, USA) was used for statistical analysis and data expression. Quantitative data with normal distribution were expressed as mean  $\pm$  standard deviation (SD). Analysis of variance was used to compare the indicators among the four groups and Tukey-Kramer method was used for *post hoc* test. Pearson's correlation analysis

was used to determine the correlation between the indicators. A  $p$ -value of  $<0.05$  was considered statistically significant.

### 3 RESULTS

#### 3.1 TICs of CEUS and parameters analysis

TICs were constructed based on the data obtained from the ROI in the center of the right liver of the four rat groups. We observed that the TIC of the 0H group rapidly reached the peak and then significantly decreased; in contrast, the TIC of the other groups slowly increased and then gradually decreased. Furthermore, the TIC increasing and decreasing trends of the 12H group were significantly slower than those of the 6H and 24H groups (Figure 1). For TIC parameters, we observed that the PI, TTP, AUC, and MTT were significantly higher in the 6H, 12H, and 24H groups than in the 0H group; these parameters were the highest in the 12H group, with a significant decrease in the parameters in 24H group compared with the 12H group ( $p < 0.05$ ). In addition, PI was significantly lower and TTP, AUC, and MTT were significantly higher in the 24H group than in the 6H group ( $p < 0.05$ ) (Figure 2).

Location for figure 1

Location for figure 2

#### 3.2 Serum biochemical test results

Figure 3 illustrates the ALT and AST levels in the four rat groups. ALT and AST levels were significantly higher in the 6H, 12H, and 24H groups than in the 0H group, with the ALT and AST levels being the highest in the 12H group ( $p < 0.05$ ). In contrast, ALT and AST levels were significantly lower in the 24H group than in the 12H group; however, AST levels were significantly lower than those in the 6H group ( $p < 0.05$ ), whereas no significant difference was observed for ALT levels ( $p > 0.05$ ).

Location for figure 3

### 3.3 mRNA expression of IL-6, NF- $\kappa$ B, and STAT3

qRT-PCR was performed to measure the mRNA expression of IL-6, NF- $\kappa$ B, and STAT3. IL-6, NF- $\kappa$ B, and STAT3 expression was higher in the 12H and 24H groups than in the 0H group, ( $p < 0.05$ ); however, no significant difference was observed in the 6H group ( $p > 0.05$ ). Furthermore, IL-6 expression was significantly lower but STAT expression was significantly higher in the 24H group than in the 12H group ( $p < 0.05$ ). Nevertheless, no significant difference was observed in NF- $\kappa$ B expression between the 12H and 24H groups ( $p > 0.05$ ) (Figure 4).

Location for figure 4

### 3.4 Histopathologic changes

HE staining for histopathologic examination of the paraffin-embedded liver tissues revealed that pathological injury in the liver tissues was characterized by hepatic steatosis and increased hematopoietic cells. Slight hepatic steatosis and a small increase in hematopoietic cells were observed in the hepatic sinusoids of the rats in the 6H group. Furthermore, hepatic lobular steatosis was observed in the 12H group. Hematopoietic cells were slightly increased in the portal area in the 24H group. Among these three groups, the injury degree was more severe in the 12H group (Figure 5).

Location for figure 5

### 3.5 Correlation analysis

Correlation analysis of the quantitative CEUS parameters with blood biochemical indicators and IL-6, NF- $\kappa$ B, and STAT3 mRNA expression revealed that STAT3 expression was positively correlated with NF- $\kappa$ B ( $r = 0.765$ ,  $p = 0.027$ ), PI ( $r = 0.813$ ,  $p = 0.014$ ), AUC ( $r = 0.875$ ,  $p = 0.005$ ), and MTT ( $r = 0.767$ ,  $p < 0.01$ ) in the 6H group. In contrast, a negative correlation was observed between AUC and ALT ( $r = -0.736$ ,  $p = 0.037$ ) but a positive correlation between AUC and MTT ( $r = 0.966$ ,  $p < 0.0001$ ) and PI ( $r = 0.903$ ,  $p = 0.002$ ). Furthermore, a negative correlation was observed between MTT and ALT ( $r = -0.819$ ,  $p =$

0.013) but a positive correlation between MTT and PI ( $r = 0.813$ ,  $p = 0.014$ ) (Figure 6). In the 24H group, positive correlations were observed between TTP and IL-6 expression ( $r = 0.710$ ,  $p = 0.049$ ), AUC and PI ( $r = 0.766$ ,  $p = 0.027$ ), and AST and ALT ( $r = 0.895$ ,  $p = 0.003$ ) (Figure 7). However, no significant correlations were observed between the parameters in the 0H and 12H groups ( $p > 0.05$ ).

Location for figure 6

Location for figure 7

#### 4 DISCUSSION

In this study, we successfully constructed a rat model of melittin-induced ALI. We observed that serum ALT and AST levels were increased in rats with a bee sting. Furthermore, histopathologic examination revealed hepatic steatosis and increased hematopoietic cells in the liver tissues. In addition, PI, TTP, AUC, and MTT of CEUS and IL-6, NF- $\kappa$ B, and STAT3 expression were significantly increased.

As markers for hepatocyte injury<sup>[27]</sup>, AST and ALT have been commonly employed in experiments to observe liver injury<sup>[9, 21, 28, 29]</sup>. Our study findings are consistent with those of a study on lipopolysaccharide/D-galactosamine/dimethyl sulfoxide-induced fulminant liver failure in mice<sup>[30]</sup>, in which rats with bee stings exhibited obvious liver damage from 6 h; this damage manifested as increased AST and ALT levels. Furthermore, hepatic steatosis and increased hematopoietic cells began to appear in this stage, which peaked at 12 h. Nevertheless, after 24 h, the liver function began to recover, with improvements in liver microcirculation. However, different from the findings of a previous study<sup>[20]</sup>, in the present study, ALT did not significantly decrease compared with that at 6 h; this may be because a negative correlation was observed between ALT and MTT and AUC. AUC can reflect blood volume and blood flow velocity in liver tissues by calculating the total amount of the microbubble contrast agent in the ROI of the liver tissues<sup>[24, 31]</sup> and the MTT of the contrast agent<sup>[32, 33]</sup>. We speculate that the improvements in ALT depend more on liver

microcirculation. When liver injury occurs, steatosis and swelling are observed in liver cells, with a decrease in liver parenchymal blood perfusion, inflammatory cell infiltration, and liver microcirculation inhibition<sup>[16]</sup>; these phenomena can affect ALT recovery. In this study, we further confirmed that early liver injury recovery can be evaluated based on liver microcirculation changes in the acute phase<sup>[18]</sup>.

In general, liver microcirculation disturbance is a vital regulatory mechanism after liver injury<sup>[13, 18]</sup>. In the present study, CEUS revealed significant liver microcirculation dysfunction in rats with acute liver injury. PI, TTP, AUC, and MTT significantly increased from 6 h after ALI. In the acute phase, swollen hepatocytes compressed the intrahepatic lumen structure, and dysfunction of liver parenchymal perfusion prolonged MTT and TTP; these findings are consistent with those of some studies on radiation-induced liver damage<sup>[16]</sup> and liver transplantation *versus* host disease<sup>[21]</sup>. Liver microcirculation can protect liver function and control inflammation<sup>[18]</sup>. For maintaining liver homeostasis, histologic examination reveals increased hematopoietic cells and hepatic blood flow, and CEUS reveals high PI and AUC. Increased hepatic arterial blood flow during the acute phase may be a marker for early recovery from liver injury<sup>[18]</sup>. In fact, the acute phase reaction of ALI generally lasts for 24–48 h, with a return to normal liver function<sup>[34]</sup>; therefore, it is a self-limited disease<sup>[13]</sup>. This trend was supported by improvements in biochemical, pathologic, and microcirculation blood perfusion measures at 24 h in our study.

Several studies have revealed that ALI is an inflammatory liver disease<sup>[10, 28, 35]</sup>. When liver injury occurs, first, the inflammatory process is triggered<sup>[8, 36]</sup>, resulting in structural and functional liver damage<sup>[37]</sup>. NF- $\kappa$ B is the most important inflammatory regulator<sup>[37]</sup>. Activation of the NF- $\kappa$ B signaling pathway increases the release of various proinflammatory factors, including IL-6<sup>[9]</sup>, triggering the accumulation of associated inflammatory cells, promoting disease progression, and maintaining liver inflammation<sup>[38]</sup>. We observed that NF- $\kappa$ B and IL-6 expression reached the peak at 12 h in rats with melittin-induced liver injury and that liver injury was the most severe; this was consistent with the results of ALT, AST, and histopathologic examination. In addition, we observed that STAT3 expression was

significantly increased; this was owing to the activation of the JAK/STAT pathway by IL-6-induced inflammation<sup>[27]</sup>. Liver protection was achieved via hepatocyte regeneration<sup>[35, 36, 39]</sup>. During the liver protection process, STAT3 is not only involved in cell proliferation during liver regeneration<sup>[40]</sup> but also in angiogenesis<sup>[38]</sup>. Liver perfusion is a major determinant of liver repair and regeneration capacity<sup>[18]</sup>. In this study, we observed a positive correlation between STAT3 expression and MMT, PI, and AUC; however, no such correlations were observed for NF- $\kappa$ B and IL-6. Interestingly, this correlation was observed at 6 h, indicating that the liver regeneration ability could be assessed based on microcirculation blood perfusion changes observed via early CEUS after bee sting injury; this has not been reported previously.

At present, owing to the small sample size of this study, we could not investigate whether the correlation between microcirculation blood perfusion and STAT3 expression remains consistent in different degrees of liver damage. Therefore, in the future, additional verification via large-sample studies is warranted.

## 5 CONCLUSION

Serum biochemical, histopathologic, and microcirculation blood perfusion changes were observed in the rat model of melittin-induced ALI. Furthermore, the early microcirculation blood perfusion changes observed via CEUS were associated with liver regeneration. Our study findings may provide a basis for evaluating the timing and effect of the anti-inflammatory treatment of bee stung-induced liver damage in clinical settings and preventing liver failure occurrence.

## ACKNOWLEDGMENTS

This research was funded by the Scientific Research Project of Jianyang People's Hospital, grant number JY202248.

## CONFLICTS OF INTEREST

none

## REFERENCES

- [1] Zheng X, Wang X, Wang Q, et al. Severe pathological changes in the blood and organs of SD rats stung by honeybees[J]. *Toxicon*, 2023,231:107196.
- [2] Yousefpoor Y, Osanloo M, Mirzaei-Parsa M J, et al. Subcutaneous Injection of Bee Venom in Wistar Rats: effects on blood cells and biochemical parameters[J]. *J Pharmacopuncture*, 2022,25(3):250-257.
- [3] Nguyen T N, Jeng M J, Chen N Y, et al. Outcomes of wasp and bee stings in Taiwan[J]. *Clin Toxicol (Phila)*, 2023,61(3):181-185.
- [4] Liu D, Fu T, Li W, et al. Efficacy of hemoperfusion combined with methylprednisolone in the treatment of heart and liver function injury caused by bee venom sting[J]. *Panminerva Med*, 2022,64(2):292-293.
- [5] Liu Z, Li X D, Guo B H, et al. Acute interstitial nephritis, toxic hepatitis and toxic myocarditis following multiple Asian giant hornet stings in Shaanxi Province, China[J]. *Environ Health Prev Med*, 2016,21(4):231-236.
- [6] Mao S, Yao J, Zhang T, et al. Bilobalide attenuates lipopolysaccharide-induced HepG2 cell injury by inhibiting TLR4-NF-kappaB signaling via the PI3K/Akt pathway[J]. *Exp Ther Med*, 2024,27(1):24.
- [7] Bala S, Zhuang Y, Nagesh P T, et al. Therapeutic inhibition of miR-155 attenuates liver fibrosis via STAT3 signaling[J]. *Mol Ther Nucleic Acids*, 2023,33:413-427.
- [8] Del C J, Gallego P, Grande L. Role of inflammatory response in liver diseases: Therapeutic strategies[J]. *World J Hepatol*, 2018,10(1):1-7.
- [9] Huang H M, Liu Y J, Fu R, et al. Protective effect of bromo- and extra-terminal domain inhibitor (+) , JQ1 on LPS / D-Gal-induced acute liver failure in mice [J]. *Prac Hepatol*, 2020,23(06):781-784.
- [10] Shen J, Kom M C, Huang H, et al. Role of NF-kappaB signaling pathway in hexavalent chromium-induced hepatotoxicity[J]. *Environ Toxicol*, 2023,38(6):1361-1371.
- [11] Moh A, Iwamoto Y, Chai G X, et al. Role of STAT3 in liver regeneration: survival, DNA synthesis, inflammatory reaction and liver mass recovery[J]. *Lab Invest*, 2007,87(10):1018-1028.
- [12] Giraldez M D, Carneros D, Garbers C, et al. New insights into IL-6 family cytokines in metabolism, hepatology and gastroenterology[J]. *Nat Rev Gastroenterol Hepatol*, 2021,18(11):787-803.

- [13] Miyazaki M, Kato M, Tanaka M, et al. Contrast-enhanced ultrasonography using Sonazoid to evaluate changes in hepatic hemodynamics in acute liver injury[J]. *J Gastroenterol Hepatol*, 2011,26(12):1749-1756.
- [14] Vollmar B, Menger M D. The hepatic microcirculation: mechanistic contributions and therapeutic targets in liver injury and repair[J]. *Physiol Rev*, 2009,89(4):1269-1339.
- [15] Emanuel A L, Meijer R I, van Poelgeest E, et al. Contrast-enhanced ultrasound for quantification of tissue perfusion in humans[J]. *Microcirculation*, 2020,27(1):e12588.
- [16] Xin T Y, Feng J, Chen S B, et al. Application of quantitative analysis of contrast-enhanced ultrasonography in the evaluation of acute radiation-induced liver damage[J]. *Exp Ther Med*, 2020,19(4):2957-2962.
- [17] Qin S, Chen Y, Wang Y, et al. Contrast-enhanced ultrasound with microbubbles containing sulfur hexafluoride and perfluorobutane with Kupffer phase for the detection of colorectal liver metastases[J]. *Eur Radiol*, 2024,34(1):622-631.
- [18] Kuroda H, Abe T, Fujiwara Y, et al. Contrast-Enhanced Ultrasonography-Based Hepatic Perfusion for Early Prediction of Prognosis in Acute Liver Failure[J]. *Hepatology*, 2021,73(6):2455-2467.
- [19] Zocco M A, Cintoni M, Ainora M E, et al. Noninvasive Evaluation of Clinically Significant Portal Hypertension in Patients with Liver Cirrhosis: The Role of Contrast-Enhanced Ultrasound Perfusion Imaging and Elastography[J]. *Ultraschall Med*, 2023,44(4):428-435.
- [20] Nan G L, Ruan X Y, Wang L, et al. Quantitative analysis of contrast-enhanced ultrasound for hepatic ischemia-reperfusion injury in rats: a experimental study [J]. *Clin Ultrasound in Med*, 2021,23(12):881-884.
- [21] Xin Y, Xiong Y, Liu F, et al. Quantitative analysis of contrast-enhanced ultrasonography in rat models of hepatic acute graft-versus-host disease[J]. *Quant Imaging Med Surg*, 2023,13(8):4908-4918.
- [22] Shu Y, Yang Y, Zhao Y, et al. Melittin Inducing the Apoptosis of Renal Tubule Epithelial Cells through Upregulation of Bax/Bcl-2 Expression and Activation of TNF-alpha Signaling Pathway[J]. *Biomed Res Int*, 2019,2019:9450368.
- [23] Dietrich C F, Nolsoe C P, Barr R G, et al. Guidelines and Good Clinical Practice Recommendations for Contrast-Enhanced Ultrasound (CEUS) in the Liver-Update 2020 WFUMB in Cooperation with EFSUMB,

- AFSUMB, AIUM, and FLAUS[J]. *Ultrasound Med Biol*, 2020,46(10):2579-2604.
- [24] Li M H, Li W W, He L, et al. Quantitative evaluation of colorectal tumour vasculature using contrast-enhanced ultrasound: Correlation with angiogenesis and prognostic significance[J]. *World J Gastrointest Surg*, 2023,15(9):2052-2062.
- [25] Zhang K, Zhang M X, Meng X X, et al. Targeting GPR65 alleviates hepatic inflammation and fibrosis by suppressing the JNK and NF-kappaB pathways[J]. *Mil Med Res*, 2023,10(1):56.
- [26] Livak K J, Schmittgen T D. Analysis of relative gene expression data using real-time quantitative PCR and the 2(-Delta Delta C(T)) Method[J]. *Methods*, 2001,25(4):402-408.
- [27] Zhou Y, Chen J, Yao Z, et al. Gastrodin ameliorates Concanavalin A-induced acute hepatitis via the IL6/JAK2/STAT3 pathway[J]. *Immunopharmacol Immunotoxicol*, 2022,44(6):925-934.
- [28] Sun L J, Chen X, Zhu S, et al. Hesperetin derivative 2a inhibits lipopolysaccharide-induced acute liver injury in mice via downregulation of circDcbl2[J]. *Acta Pharmacol Sin*, 2024,45(2):354-365.
- [29] Tian W S, Zhao J, Kim M K, et al. Veronica persica ameliorates acetaminophen-induced murine hepatotoxicity via attenuating oxidative stress and inflammation[J]. *Biomed Pharmacother*, 2023,169:115898.
- [30] Alhareth D Y, Alanazi A, Alanazi W A, et al. Carfilzomib Mitigates Lipopolysaccharide/D-Galactosamine/Dimethylsulfoxide-Induced Acute Liver Failure in Mice[J]. *Biomedicines*, 2023,11(11).
- [31] Xin T Y, Feng J, Chen S B, et al. Application of quantitative analysis of contrast-enhanced ultrasonography in the evaluation of acute radiation-induced liver damage[J]. *Exp Ther Med*, 2020,19(4):2957-2962.
- [32] Li H, Lu J, Zhou X, et al. Quantitative Analysis of Hepatic Microcirculation in Rabbits After Liver Ischemia-Reperfusion Injury Using Contrast-Enhanced Ultrasound[J]. *Ultrasound Med Biol*, 2017,43(10):2469-2476.
- [33] Jung E M, Weber M A, Wiesinger I. Contrast-enhanced ultrasound perfusion imaging of organs[J]. *Radiologe*, 2021,61(Suppl 1):19-28.
- [34] Schmidt-Arras D, Rose-John S. IL-6 pathway in the liver: From physiopathology to therapy[J]. *J Hepatol*, 2016,64(6):1403-1415.

- [35] Deng C, Hu J, He L, et al. Daucosterol combined with umbilical cord mesenchymal stem cell-derived exosomes can alleviate liver damage in liver failure mice by regulating the IL-6/STAT3 signaling pathway[J]. *Cancer Biol Ther*, 2023,24(1):2184150.
- [36] Di-Iacovo N, Pieroni S, Piobbico D, et al. Liver Regeneration and Immunity: A Tale to Tell[J]. *Int J Mol Sci*, 2023,24(2).
- [37] Mao S, Yao J, Zhang T, et al. Bilobalide attenuates lipopolysaccharide-induced HepG2 cell injury by inhibiting TLR4-NF-kappaB signaling via the PI3K/Akt pathway[J]. *Exp Ther Med*, 2024,27(1):24.
- [38] Li J, Wu B, Zeng L, et al. Aqueous extract of *Amydrium sinense* (Engl.) H. Li alleviates hepatic fibrosis by suppressing hepatic stellate cell activation through inhibiting Stat3 signaling[J]. *Front Pharmacol*, 2023,14:1101703.
- [39] Giraldez M D, Carneros D, Garbers C, et al. New insights into IL-6 family cytokines in metabolism, hepatology and gastroenterology[J]. *Nat Rev Gastroenterol Hepatol*, 2021,18(11):787-803.
- [40] Zou S, Tong Q, Liu B, et al. Targeting STAT3 in Cancer Immunotherapy[J]. *Mol Cancer*, 2020,19(1):145.

Table 1 Rat primer sequences for qRT-PCR.

Gene	Direction	Sequences (5'-3')	Gene ID	Product length_(bp)
GAPDH	Forward	ACAGCAACAGGGTGGTGGAC	24383	226
	Reverse	TTTGAGGGTGCAGCGAACTT		
NF-κB	Forward	GGATGGCTTCTATGAGGCTGAACTC	309165	98
	Reverse	CTTGCTCCAGGTCTCGCTTCTTC		
IL-6	Forward	ACTTCCAGCCAGTTGCCTTCTTG	24498	110
	Reverse	TGGTCTGTTGTGGGTGGTATCCTC		
STAT3	Forward	TGAGGGAGCAGAGATGTGGG	25125	144
	Reverse	CTGGCAAGGAGTGGGTCTCT		

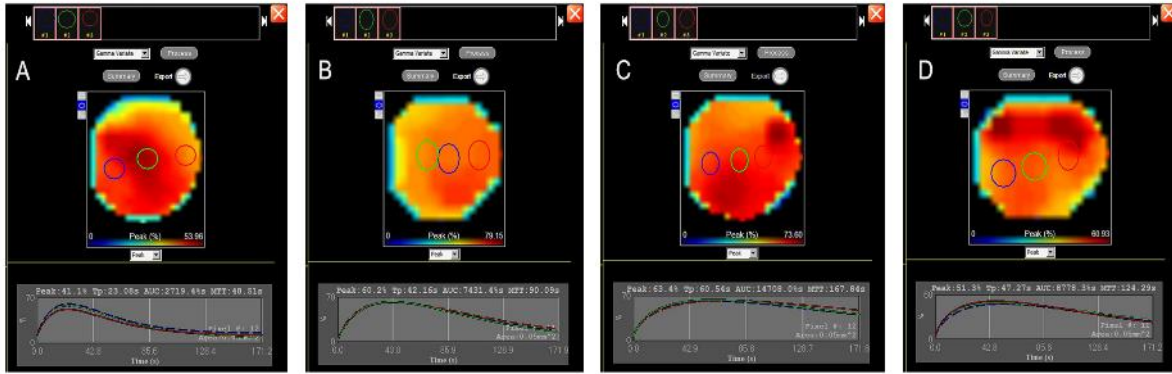


Figure 1 TICs of the CEUS imaging of the rats in the four groups

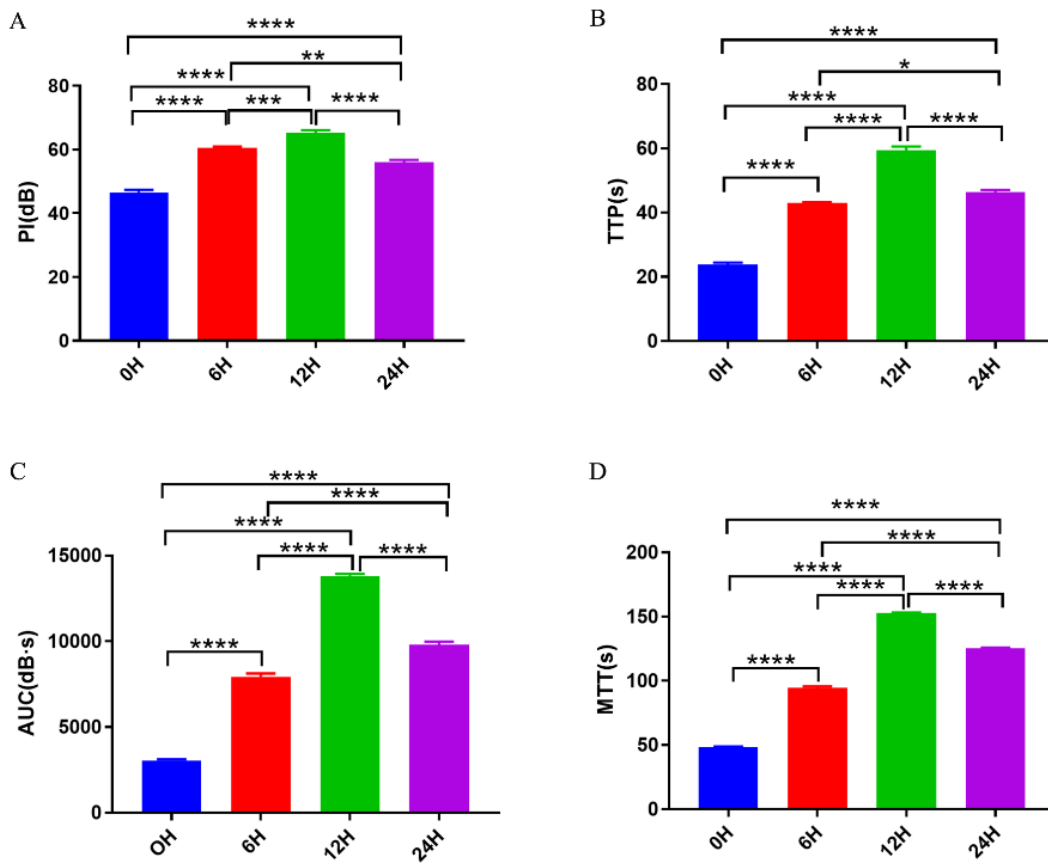


Figure 2 Comparison of the TIC parameters of contrast-enhanced ultrasound of the four rat groups: the mean and standard deviation of PI (A), TTP (B), AUC (C), and MTT (D). \*\*\*\*,  $p < 0.0001$ ; \*\*\*,  $p < 0.001$ ; \*\*,  $p < 0.01$ ; and \*,  $p < 0.05$ . PI, peak intensity; TTP, time to peak; AUC, area under the curve; MTT, mean transition

time.

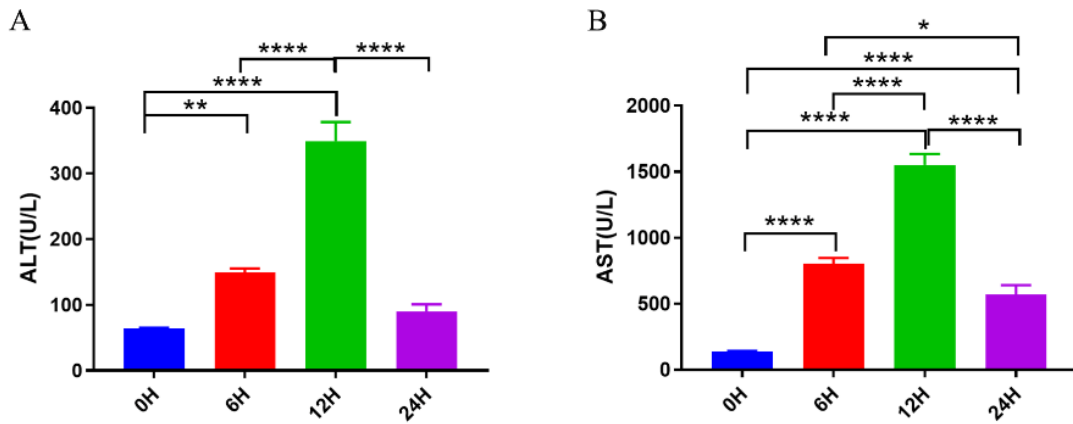


Figure 3 Comparison of serum ALT (A) and AST (B) levels among the four rat groups. \*\*\*\*  $p < 0.0001$ ; \*\*  $p < 0.01$ ; and \*  $p < 0.05$ . AST, aspartate aminotransferase; ALT, alanine aminotransferase.

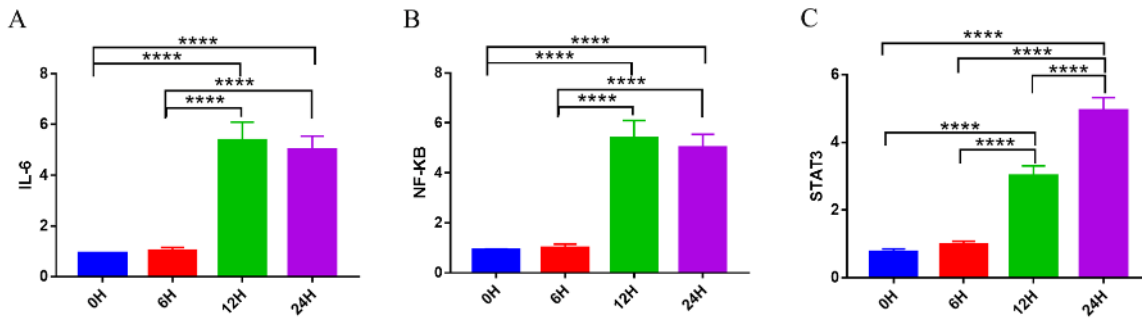


Figure 4 Comparison of the mRNA expression of IL-6 (A), NF-κB (B), and STAT3 (C) in the liver tissues of the four rat groups. \*\*\*\*,  $p < 0.0001$ . IL-6, interleukin-6; NF-κB, nuclear factor kappa B; STAT3, signal transducer and activator of transcription 3.

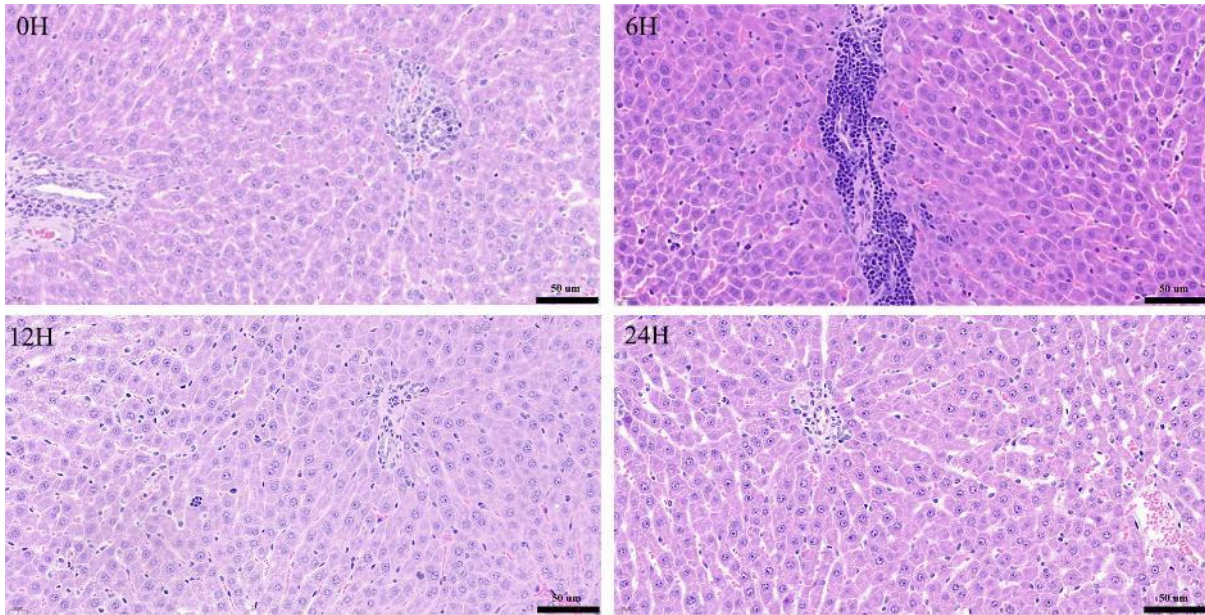


Figure 5 Hematoxylin–eosin (HE) staining results (×400) of the liver tissues of the rats in each group. The nuclei are stained blue and the cytoplasm is stained red.

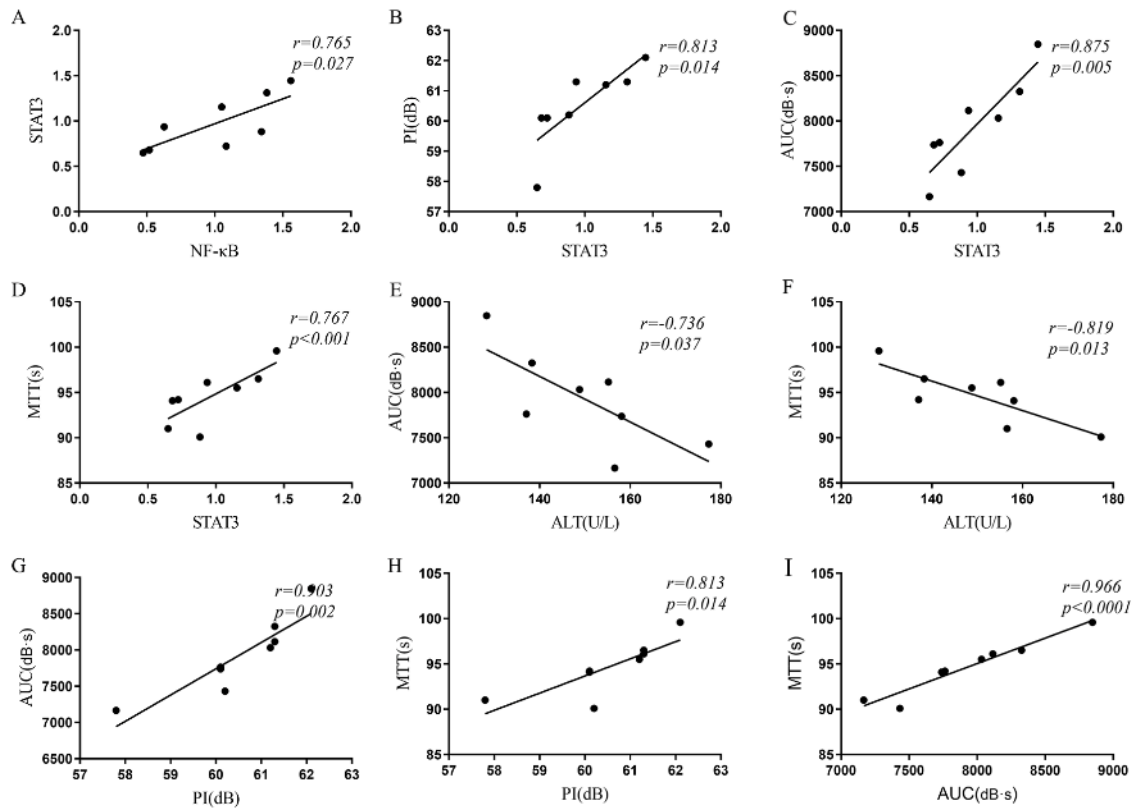


Figure 6 Correlation analysis of the TIC parameters of contrast-enhanced ultrasound with biochemical indexes and immunohistochemical results in the 6H group. A, Correlation between STAT3 and NF-κB expression. B, Correlation between STAT3 expression and PI. C, Correlation between STAT3 expression and AUC. D, Correlation between STAT3 expression and MTT. E, Correlation between AUC and ALT. F, Correlation between

MTT and ALT. G, Correlation between AUC and PI. H, Correlation between MTT and PI. I, Correlation between AUC and MTT. ALT, alanine aminotransferase; PI, peak intensity; AUC, area under the curve; MTT, mean transition time; NF- $\kappa$ B, nuclear factor kappa B; STAT3, signal transducer and activator of transcription 3.

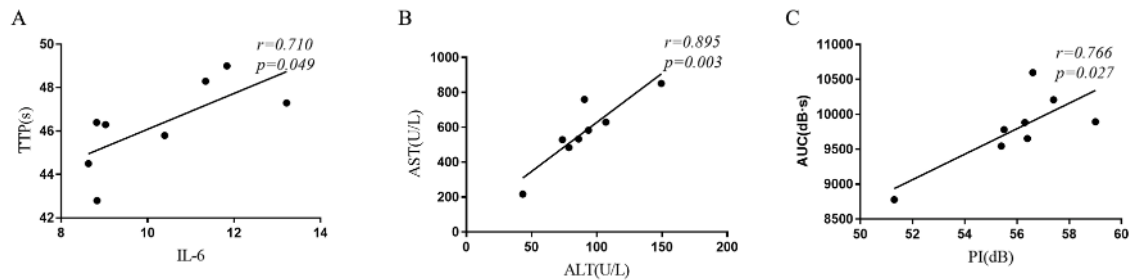


Figure 7 Correlation analysis of CEUS TIC parameters with serum biochemical indexes and mRNA expression in the 24H group. A, Correlation between TTP and IL-6 expression. B, Correlation between AST and ALT. C, Correlation between AUC and PI. PI, peak intensity; TTP, time to peak; AUC, area under the curve; IL-6, interleukin-6; ALT, alanine aminotransferase; AST, aspartate aminotransferase.

#### Corresponding Author:

Mingxing LI

Department of Ultrasound, The Affiliated Hospital of Southwest Medical University, Luzhou 646000, China

E-MAIL: lmx526@sina.com